Title: Pebble Flow and Coolant Flow Analysis Based on a Fully Coupled Multiphysics Model

Authors: Yanheng Li and Wei Ji*

Department of Mechanical, Aerospace, and Nuclear Engineering
Rensselaer Polytechnic Institute
110 8th Street, Troy, NY 12180-3590 USA
*jiw2@rpi.edu

Abstract --- In pebble bed reactors (PBRs), pebble flow and coolant flow are highly correlated, and the behavior of each flow is strongly influenced by pebble-coolant interactions. Simulation of both flows in PBRs presents a multiphysics computational challenge because of the strong interplay between the flows. In this paper, a fully coupled multiphysics model is developed and applied to analyze the pebble flow and coolant flow in helium gas-cooled and fluoride salt-cooled PBR designs. A discrete element method is used to simulate the pebble motion to obtain the distribution of pebble density and velocity and the maximum contact stress on each pebble. Computational fluid dynamics is employed to simulate coolant dynamics to obtain the distribution of coolant velocity and pressure. The two methods are fully coupled through the calculation and exchange of pebble-coolant interactions at each time step. Thus, a fully coupled multiphysics computational framework is formulated. A scaled experimental fluoride salt-cooled reactor facility and a full-core helium gas-cooled HTR-10 reactor are simulated. Noticeable changes, such as higher pebble density in the cylindrical core region and more uniform vertical fluid speed profile due to the coupling effect, are observed compared to previous single-phase alone simulations without coupling. These changes suggest that the developed computational framework has higher fidelity compared with previous uncoupled methodology in analyzing pebble flow in PBRs. For the scaled experimental fluoride salt-cooled reactor facility calculation, similar hydraulic loss can be obtained as measured in the University of California, Berkeley, Pebble Recirculation Experiment (PREX), demonstrating the potential of the developed method in thermal-hydraulic analysis for PBRs.

Keywords: Pebble Bed Reactors, Discrete Element Method and Computational Fluid Dynamics, Multi-Physics Coupling

I. INTRODUCTION

Pebble bed reactor (PBR) designs, including pebble bed very high temperature gas-cooled reactors[1] and pebble bed advanced high temperature reactors (PB-AHTR),[2,3] are promising future-generation reactors with inherently passive safety, high energy efficiency, and flexible online refueling capability. These features root in their unique fuel designs and operation characteristics: tens or hundreds of thousands of fuel pebbles are circulating through reactor core regions, forming

granular-flow pebble bed. Gas or liquid coolant passes through densely packed pebbles to bring fission heat out for electricity generation. To provide highly reliable safety assessment for PBR designs, one has to track the motions of each pebble and its surrounding coolant flow to obtain the realistic distribution of pebbles for full-core neutronic and thermal-hydraulic analysis under transient, normal and off-normal operation conditions.[1-4] It is clear that a highly accurate and efficient pebble flow simulation is important for accurate full-core analysis.

Pebble flow and coolant flow in a PBR can be considered a dense time-varying fluid-particle system, in which pebble flow is a discrete solid particle phase and coolant flow is a continuum fluid phase. The pebble motion is governed by forces from pebble gravity, pebble-pebble and wall-pebble contacts, and coolant-pebble interactions. Coolant is driven into the reactor core at high pressure and passes through the gaps between pebbles, forming a porous medium configuration in the pebble bed. Because of the viscosity and pressure gradient, the major interactions between coolant and pebble are drag and pressure gradient forces. Existing work on the PBR dynamics simulation focuses on single-phase study; i.e. the pebble flow and the coolant flow were studied separately without pebble-coolant coupling.[5-7] Pebble flow was simulated using either a discrete element method[8] (DEM) or modified molecular dynamics method,[9] accounting for the contact forces between the pebbles and between pebbles and reactor wall. After the pebble distribution was obtained, the position of each pebble was passed to other multiphysics analysis codes to perform neutronic and thermal-hydraulic computations,[7] in addition to safety-related analysis, including earthquake impact analysis.[4] However, no coolant-pebble interaction has been accounted for in the previous pebble flow simulation work.

In practice, there is a strong interplay between pebble flow and coolant flow in typical PBR designs. For example, in a helium gas-cooled PBR, such as PBMR-400 (Ref. 10), high-speed helium gas passes through the void space between pebbles and exerts a strong drag force on pebbles due to viscous stress between gas and pebble. Another example is the PB-AHTR (Refs. 2 and 3), where low-speed molten salt coolant flows through pebbles, exerting a strong pressure gradient/buoyancy force so that pebbles can float and move upward to the outlet at the top of the core region. These strong forces on the pebbles inevitably affect the pebble flow by changing the pebble distribution, adding to the effects from pebble-pebble interactions. The change in spatial distribution of pebbles can also affect the coolant flow dynamics because of the change in local porosity. Thus, the pebble flow and coolant flow are strongly coupled, and the coolant-pebble interaction must be accounted for when one simulates pebble flow in PBRs.

To provide high-fidelity simulation capability in PBR analysis, especially for predicting pebble and coolant dynamics, we implement a multiphysics model that fully couples pebble flow and coolant flow simulations and apply it to analyze pebble motion and coolant velocity/pressure variations in PBRs. The motion and rotation of pebbles are simulated using DEM with contact mechanics models incorporated for pebble-pebble and wall-pebble friction and elastic interactions. A drag or buoyancy force from coolant is accounted for in the pebble flow simulation at each DEM time

step. An experimentally determined empirical model for drag law,[11-13] associated with local coolant porosity, local coolant velocity, and Reynolds number and pebble velocity, is used. Coolant flow is simulated by a high-fidelity computational fluid dynamics (CFD) method based on local averaged Navier–Stokes (N-S) equations for fluid-solid phase.[12-16] The CFD method can provide higher accuracy than the traditional porous medium approach based on Darcy's law, which is used widely for low-Reynolds-number fluid flowing through porous media.[14] The tight coupling of the pebble flow simulation and the coolant flow simulation is implemented by exchanging parameters, such as pebble porosity/velocity and coolant velocity, at each time step. The drag or buoyancy force is the coupling term that is updated and used for each flow simulation. Thus, a tightly coupled DEM-CFD computation framework is formed.

In this paper, the coupled DEM-CFD methodology is implemented and applied to model the pebble and coolant flow in two typical PBR designs. The first one is a scaled experimental PB-AHTR design facility,[3] which represents typical fluoride salt-cooled PBR designs, and the second is the HTR-10 reactor design, which represents typical gas-cooled PBR designs.[17] In the scaled experimental PB-AHTR facility, pebbles are loaded from the bottom of the core and move upward due to the higher density of coolant than pebble, and fluoride-salt coolant is circulating along the same direction. The major interaction between coolant and pebble in this design is the buoyancy force. In the HTR-10, pebbles move downward from top to the bottom, and helium gas passes through the pebble bed along the same direction at high speed. The major interaction between coolant and pebble is the drag force. In the simulation for both configurations, pebbles' moving trajectory, velocity distribution, density profile, and the maximum contact stress on each pebble are calculated. These characteristic properties are the key elements in understanding the pebble flow behavior in PBRs. On the other hand, coolant velocity and pressure distribution are important dynamic behaviors of coolant flow in PBRs and are also investigated by the coupled methodology.

The simulation results are compared with those by single-flow simulation alone without coupling. Significant changes are observed, such as a higher pebble packing state in the cylindrical core region that is much closer to the random jamming state than those observed in the pebble-flow-only situation,[5] which demonstrates the necessity of the coupling between pebble flow and coolant flow. Moreover, comparisons with experimental measurements are made, such as the hydraulic loss in the scaled PB-AHTR facility. Very close hydraulic loss value is obtained compared with the PREX experiment conducted by UC-Berkeley, which demonstrates the excellent prediction capability of the developed fully coupled multi-physics model and shows a great potential in the application of the thermal-hydraulic analysis.

The remainder of the paper is organized as follows. Section II describes in detail the governing equations, models and correlations of associated physical forces that are used for pebble and coolant flow simulation. The coupling strategy between the DEM and CFD methods and numerical simulation implementation are addressed. Section III shows the applications of the

implemented methodology to the pebble flow and coolant flow simulation in the scaled PB-AHTR facility and full-core HTR-10 configurations. The simulation results and analysis for both designs are presented. Section IV concludes the paper.

II. DESCRIPTION OF MATHEMATICAL MODELS

II.A. Governing Equations for Pebble Motion

The computation of the dynamics for a large number of pebbles can be generalized as a granular material simulation. Equations (1) and (2) are the equations of motion for the pebbles:

$$m_i \frac{d\mathbf{v}_i}{dt} = \boldsymbol{F}_i = \sum_{\substack{j \neq i \\ j=1}}^{N} \boldsymbol{F}_{ij} + \boldsymbol{W}_i + m_i \boldsymbol{g} + \boldsymbol{F}_{f,i} \tag{1}$$

and

$$J_i \frac{d\boldsymbol{\omega}_i}{dt} = \boldsymbol{T}_i, \tag{2}$$

where $\mathbf{v}_i$ is the velocity of the i^{th} pebble, $\boldsymbol{F}_i$ is the net force on the i^{th} pebble including $\boldsymbol{F}_{ij}$ the contact force from the j^{th} pebble, $\boldsymbol{W}_i$ the contact force on the i^{th} pebble from the wall, $m_i\boldsymbol{g}$ the gravitational force, and $\boldsymbol{F}_{f,i}$ the fluid-pebble interaction force, which is a function of local fluid velocity $\mathbf{u}$, pebble velocity $\mathbf{v}_i$ and local porosity ε. For gaseous fluid, $\boldsymbol{F}_{f,i}$ approximately equals the fluid drag force $\boldsymbol{F}_{D,i}$ plus the virtual mass force $\boldsymbol{F}_{VM,i}$. $\boldsymbol{T}_i$ is the torque on i^{th} pebble due to the tangential contact (shear) force, and J_i is the moment of inertia and $\boldsymbol{\omega}_i$ is the angular velocity.

The pebble-pebble contact force $\boldsymbol{F}_{ij}$ consists of two components: normal contact force $\boldsymbol{F}_{\text{n},ij}$ and tangential contact force $\boldsymbol{F}_{\text{t},ij}$. Several models have been proposed and studied to mathematically express the contact forces.[19] Among these models, due to high accuracy, the model of Hertzian contact law/nonlinear spring with energy dissipation is chosen in this paper for the normal contact force computation. Also, the stick-slip model, which is dependent on the contact history, is chosen for tangential contact forces. [18,19]

According to contact mechanics,[18,19] the normal contact force $\boldsymbol{F}_{\text{n},ij}$ between two spheres i and j with radius r_i, r_j and velocity $\mathbf{v}_i$, $\mathbf{v}_j$ is given by

$$\boldsymbol{F}_{\text{n},ij} = \sqrt{\frac{r_i r_j}{r_i + r_j}} \left(k_{\text{n}} \delta_{ij}^{\ 1.5} - \gamma_{\text{n}} \delta_{ij}^{\ 0.5} \, \text{v}_{\text{n},ij} \right) \mathbf{n}_{ij}, \tag{3}$$

where k_{n} and γ_{n} are material elastic and viscoelastic constants respectively, $\text{v}_{\text{n},ij}$ is the relative normal speed defined as $(\mathbf{v}_i\text{-}\mathbf{v}_j)\cdot\mathbf{n}_{ij}$, $\mathbf{n}_{ij}$ is the unit normal vector pointing from the center of pebble i to the center of pebble j, and δ_{ij} is the overlap size.

For the tangential contact force, the stick-slip model[18,19] is used combined with Coulomb's dry friction law:

$$\boldsymbol{F}_{\text{t},ij} = -k_{\text{t}} \delta_{ij}^{\ 0.5} \int_{t_0}^{t} \mathbf{v}_{\text{t},ij} dt, \ \left\| \boldsymbol{F}_{\text{t},ij} \right\| \leq \mu \left\| \boldsymbol{F}_{\text{n},ij} \right\|, \tag{4}$$

where k_t is the tangential elastic constant, and $\mathbf{v}_{t,ij}$ is the relative tangential velocity defined as $\mathbf{v}_i - \mathbf{v}_j - [(\mathbf{v}_i - \mathbf{v}_j)\cdot\mathbf{n}_{ij}]\mathbf{n}_{ij} + \frac{r_i\boldsymbol{\omega}_i \times (d_{ij}\mathbf{n}_{ij}) + r_j\boldsymbol{\omega}_j \times (d_{ij}\mathbf{n}_{ij})}{r_i + r_j}$, where d_{ij} is the distance between the center of sphere i and the center of sphere j.

The wall-pebble contact force $\boldsymbol{W}_i$ follows the same models as used in the pebble-pebble contact. The normal wall contact force $\boldsymbol{W}_{n,i}$ is written as

$$\boldsymbol{W}_{n,i} = \sqrt{r_i}(k_n \delta_{w,i}^{1.5} - \gamma_n \delta_{w,i}^{0.5} v_{nw,i})\mathbf{n}_{wi}. \quad (5)$$

where $v_{nw,i}$ is the normal component of pebble speed relative to the wall, defined as $\mathbf{v}_i \cdot \mathbf{n}_{wi}$, $\mathbf{n}_{wi}$ is the unit normal vector pointing from the pebble-wall contact point to the center of pebble i, and $\delta_{w,i}$ is the overlap size with the wall.

The tangential wall contact force $\boldsymbol{W}_{t,i}$ can be expressed as

$$\boldsymbol{W}_{t,i} = -k_t \delta_{w,i}^{0.5} \int_{t_0}^{t} \mathbf{v}_{tw,i} dt, \ \left\|\boldsymbol{W}_{t,i}\right\| \le \mu \left\|\boldsymbol{W}_{n,i}\right\|, \quad (6)$$

where $\mathbf{v}_{tw,i}$ is the tangential component of pebble velocity relative to the wall, defined as $\mathbf{v}_i - (\mathbf{v}_i \cdot \mathbf{n}_{wi})\mathbf{n}_{wi} - r_i\boldsymbol{\omega}_i \times \mathbf{n}_{wi}$.

The fluid-pebble force $\boldsymbol{F}_{f,i}$ represents the forces that are exerted onto the pebble from the fluid, such as the drag force caused by the relative motion between pebble and fluid due to the viscosity. Besides drag force, other forces may also be significant, such as the buoyancy force due to the pressure gradient, the Magnus force due to pebble rotation, the virtual mass force due to pebble motion acceleration, and the Saffman force due to the fluid velocity gradient.[13] In the case of dense and slow-moving granular flow, the primary interaction forces are the drag force, the buoyancy (for liquid fluid only), and the virtual mass force. The calculation of these forces is related to the surrounding fluid properties and the local pebble packing fraction around the pebble in question, which will be discussed in detail in Sec. II.C.

In the discrete element model, the consecutive movement of individual pebbles is simulated based on Newton's second law of motion. Explicit finite difference-based integration of Eqs. (1) and (2) is performed combined with the force and torque calculation in each time step to give the translational and rotational displacements of each pebble.

In each time step, the translational and rotational acceleration for each pebble due to the net force $\boldsymbol{F}_i$ and torque $\boldsymbol{T}_i$ are calculated using Eqs. (1) and (2). These values are assumed constant over each time step, and after the integration calculation, the new velocities and new positions are obtained. From the new positions, the overlaps between contacting pebbles and the consequent contact forces are evaluated. A vector summation of all forces is used in the next time step to obtain new values of $\boldsymbol{F}_i$ and $\boldsymbol{T}_i$. Pebble-wall interactions are treated in the same way as pebble-pebble interactions except that the wall is fixed.

The time step is determined based on previous analysis of DEM by other researchers, such as

Cundall and Strack[8] and Mishra and Murty[20]. In their work, a critical (maximum) time step for DEM is determined as $\Delta t_c = C\sqrt{m / K_{\mathrm{n}}}$, where K_{n} is the contact stiffness,[20] and C is a numerical constant, which is typically chosen as a value from 0.2 (Ref. 20) to 2 (Ref. 8). To achieve high efficiency and guarantee the stability of the numerical scheme, the time step Δt is taken as a value close to the critical time step. In practice, the DEM time step indeed depends on specific problems. For the studied PB-AHTR and HTR-10 applications, their critical time steps are close to each other. For PB-AHTR application, m = 7.23 g and K_{n} = 1.65 x 10^7N/m; hence Δt_c = 1.25 x 10^{-5} s. For HTR-10 application, m = 210 g and K_{n} = 2.54 x 10^8 N/m, which yields Δt_c=1.73 x 10^{-5}s. We choose a moderate C=0.6 in both PB-AHTR and HTR-10 applications. Based on these estimations and selections, a time-step size Δt = 10^{-5} s is chosen for both applications.

II.B. Governing Equations for Fluid Motions

Modeling of the fluid in a multiphase flow environment, such as the pebble flow and coolant flow in PBRs, is based on applying the time and space averaging techniques to transient conservation equations for the fluid phase.[21] In the standard CFD modeling, the numerical solution of N-S equations is needed. The locally averaged N-S equations for the fluid phase in a fluid cell are[13]

$$\frac{\partial \varepsilon \rho_f}{\partial t} + \nabla \cdot (\varepsilon \rho_f \mathbf{u}) = 0 \tag{7}$$

and

$$\frac{\partial \varepsilon \rho_f \mathbf{u}}{\partial t} + \nabla \cdot (\varepsilon \rho_f \mathbf{u}\mathbf{u}) = -\varepsilon \nabla p + \nabla \cdot \varepsilon \mu_f \nabla \mathbf{u} + \boldsymbol{f}_{\mathrm{P}} + \varepsilon \rho_f \boldsymbol{g}, \tag{8}$$

where ε is the average porosity in a fluid cell, ρ_f is the average fluid density in a fluid cell, μ_f is the fluid molecular viscosity**,** $\mathbf{u}$ is the average fluid velocity in a fluid cell, and p is the average fluid pressure. $\boldsymbol{f}_{\mathrm{P}}$ is the total force density that is exerted on the fluid by all the pebbles that fall into the fluid cell. Accurately calculating the pebble-fluid term $\boldsymbol{f}_{\mathrm{P}}$ plays a very important role in obtaining accurate solutions from the CFD computation and, consequently, has direct impact on the DEM-CFD overall accuracy and efficiency.[15] To account for pebbles residing within multiple fluid cells, a high-fidelity approach based on the particle-source-in-cell method is used in this paper to calculate $\boldsymbol{f}_{\mathrm{P}}$ in each fluid cell[15]:

$$\boldsymbol{f}_{\mathrm{P},k} = -\sum_{i \in fluid\ cell\ k} \alpha_{i,k} \boldsymbol{F}_{f,i} / V_{f,k}, \tag{9}$$

where $\alpha_{i,k}$ is the volume fraction of the i^{th} pebble that falls into the k^{th} fluid cell and $V_{f,k}$ is the volume of the k^{th} fluid cell. Equation (9) shows that the pebble-fluid force equals the summation of the fluid-pebble force on each pebble in a fluid cell, which obeys Newton's third law and relates $\boldsymbol{f}_{\mathrm{P}}$ to $\boldsymbol{F}_f$ on each pebble in one fluid cell. Because of the correlation of these two forces, the fluid phase and solid phase are coupled together, forming a two-way coupled DEM-CFD computational model. The

accuracy of these two interaction forces determines the overall computation fidelity of the coupling DEM-CFD model. Details of this coupling model will be described in Sec. II.C.

By calculating $\alpha_{i,k}$, the force from a pebble that is partially located in a fluid cell can be accurately accounted for. Meanwhile, the average porosity in the k^{th} fluid cell can be calculated by

$$\varepsilon_k = 1 - \left(\sum_{i \in fluid\ cell\ k} \alpha_{i,k} V_{\mathrm{P},i} \right) / V_{f,k}\,, \tag{10}$$

where $V_{\mathrm{P},i}$ is the volume of the i^{th} pebble. To optimize the simulation performance and reach a good trade-off between fidelity and efficiency, the typical dimension of fluid cell is chosen to be three times the pebble diameter. Hence, 20 to 30 pebbles are distributed in a fluid cell.

A semi-implicit finite volume method with staggered grids is used to discretize the incompressible N-S equations on a three-dimensional cylindrical coordinate system. Patanker's Semi-Implicit Method for Pressure Linked Equations (SIMPLE)[22] is employed to obtain the pressure and the velocity iteratively.

II.C. Coupling Terms and Strategies

As mentioned above, for pebble-coolant modeling, the major fluid-particle interaction can be approximately expressed as

$$\boldsymbol{F}_{f,i} = -V_{\mathrm{P},i} \nabla p + \boldsymbol{F}_{D,i} + \boldsymbol{F}_{VM,i}, \tag{11}$$

where $\boldsymbol{F}_{D,i}$ and $\boldsymbol{F}_{VM,i}$ are the drag force and virtual mass force acting on the i^{th} pebble .

For an isolated pebble, the drag force $\boldsymbol{F}_{D,i}$ can be written as[12]

$$\boldsymbol{F}_{D,i} = \frac{1}{2} \rho_{f,i} (\mathbf{u}_i - \mathbf{v}_i) \left\| \mathbf{u}_i - \mathbf{v}_i \right\| C_{D,i} \pi r_i^2, \tag{12}$$

where $C_{D,i}$ is the drag coefficient of the single pebble, which can be expressed by the empirical formulation[13]

$$C_{D,i} = \begin{cases} 24(1 + 0.15\,\mathrm{Re}_i^{\,0.687}) / \mathrm{Re}_i & \mathrm{Re}_i < 1000, \\ 0.44 & \mathrm{Re}_i > 1000. \end{cases} \tag{13}$$

The local Reynolds number for the fluid around the i^{th} pebble Re_i satisfies $\mathrm{Re}_i = 2\rho_{f,i} r_i \varepsilon_i \|\mathbf{u}_i - \mathbf{v}_i\| / \mu_f$, where ε_i, $\rho_{f,i}$ and $\mathbf{u}_i$ are the local porosity, fluid density, and fluid velocity around the i^{th} pebble, respectively. To achieve high accuracy in the calculation of the Reynolds number and the consequent drag coefficient, local porosity ε_i is evaluated based on the ratio of a single pebble volume $V_{\mathrm{P},i}$ to the Voronoi cell volume around the pebble.[5] Other fluid-related quantities such as $\mathbf{u}_i$ and $\rho_{f,i}$ are calculated based on the particle-source-in-cell method used in Eq. (9). As an approximation, it can be assumed ε_i, $\rho_{f,i}$ and $\mathbf{u}_i$ equal the average quantities ε, ρ and $\mathbf{u}$, respectively, in the fluid cell inside which the pebble center falls.

In the pebble bed, pebbles are stacked on each other in the fluid. The prediction of the drag force on each pebble based on Eq. (12) becomes inaccurate due to the effect of surrounding pebbles.

Various approximations and correlations have been proposed to seek accurate predictions. In this work, the voidage function presented by Di Felice[12] is employed to calculate the drag force on each pebble:

$$\boldsymbol{F}_{D,i} = \frac{1}{2}\rho_{f,i}(\mathbf{u}_i - \mathbf{v}_i)\left\|\mathbf{u}_i - \mathbf{v}_i\right\| C_{D,i}\pi r_i^2 \beta(\varepsilon_i), \tag{14}$$

where $\beta(\varepsilon_i) = \varepsilon_i^{-\{4.7-0.65\exp[-(1.5-\log \mathrm{Re}_i)^2/2]\}}$.

The virtual mass force can be described as: [13]

$$\boldsymbol{F}_{VM,i} = C_{VM} V_{\mathrm{P},i}\rho_{f,i}\left(\frac{\partial \mathbf{u}_i}{\partial t} + \mathbf{u}_i \cdot \nabla \mathbf{u}_i - \frac{\partial \mathbf{v}_i}{\partial t} - \mathbf{v}_i \cdot \nabla \mathbf{v}_i\right), \tag{15}$$

where C_{VM} is the virtual mass effect coefficient.

For each time step of the CFD solver, the pebble velocities and positions from the DEM solver are used to first calculate the cell porosity based on Eq. (10). Then, from Eqs. (14), (15) and (9), the drag force $\boldsymbol{F}_{D,i}$, virtual mass force $\boldsymbol{F}_{VM,i}$ and pebble-fluid interaction $\boldsymbol{f}_{\mathrm{P}}$ are expressed as the functions of fluid velocity **u** and pressure p. By applying these interaction terms in the averaged N-S Eqs. (7) and (8) and solving Eqs. (7) and (8) numerically, the fluid quantities **u** and p can be obtained. Consequently, the fluid-pebble interaction terms $\boldsymbol{F}_f$ and $\boldsymbol{f}_{\mathrm{P}}$ can be evaluated explicitly. These calculated fluid-pebble forces will be exported back to the DEM solver to solve the next-step pebble position $\boldsymbol{X}'$ and velocity $\mathbf{v}'$. It can be shown that, from the description of the DEM-CFD approach, there is two-way data exchange between the DEM solver and the CFD solver, as illustrated in Fig. 1.

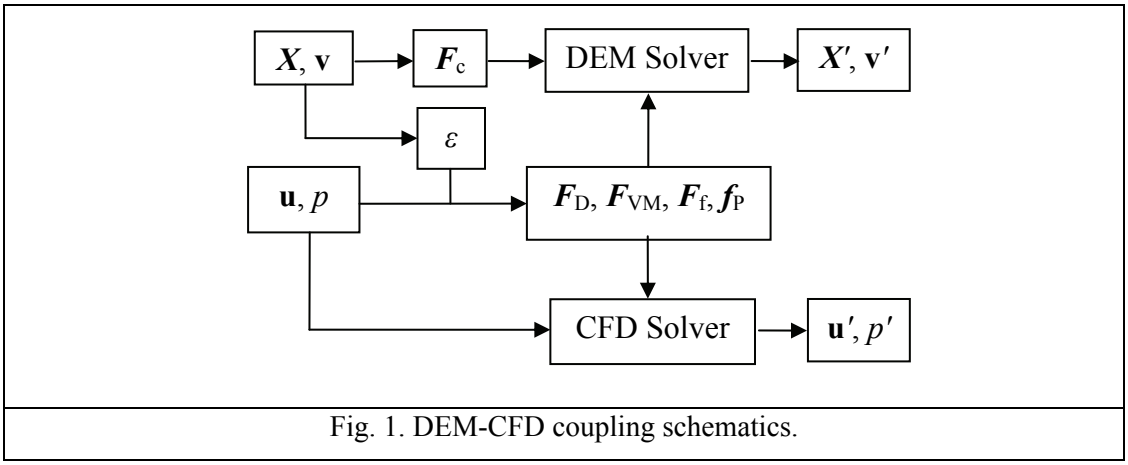

Fig. 1. DEM-CFD coupling schematics.

As discussed in Sec. II. A, a DEM time step of Δt(DEM) = 10^{-5} s is used in both PB-AHTR and HTR-10 applications. To keep high fidelity in each flow simulation while keeping a certain efficiency in overall computation, we require that the DEM and CFD solvers exchange data for every 100 DEM steps, and the pebble positions, velocities and consequent fluid cell porosities are assumed constant in the CFD solver between two exchanges. This leads to a CFD time step of Δt(CFD) = 10^{-3} s.

III. PEBBLE FLOW AND COOLANT FLOW ANALYSIS FOR PBR DESIGNS

III.A. PB-AHTR Design Simulation

In the PB-AHTR design,[2] pebbles are floating upward because the fluoride salt coolant has higher density than the fuel pebbles . This requires fuel loading at the bottom and defueling at the top in the reactor core. Several experiments have been performed to show the pebble injection loading, pebble upward landing, and pebble defueling process in a scaled facility , such as PREX conducted by UC-Berkeley, which used polypropylene-made simulant pebbles and water as simulant coolant. These two materials present the same actual coolant- pebble density ratio. In this paper, PREX geometry and material properties are used in the pebble and coolant flow simulation to demonstrate the capability of the coupled DEM-CFD approach.

The scaled reactor core in the simulation model has an inner radius of 20 cm and a height of 99.06 cm, with a 45-deg conic top cap and cylindrical chute. On the wall of the conic top, there are pore holes that account for one-fourth of the conic wall area, which can facilitate the outflow of water. A total of 8300 pebbles are loaded and randomly distributed within the core at a packing fraction of ~62%. During the recirculation, pebbles are injected from the bottom of the core, travel through the core, and are removed from the top of the chute. Meanwhile, water (simulant coolant) enters from the bottom of the reactor and leaves from the top of the reactor, with the boundary conditions of constant velocity inlet and constant pressure outlet. The geometry is shown in Fig. 2a, and the physical parameters for the pebbles and coolant are listed in Table I.

Table I Material Physical Properties in PREX

Pebble	Radius	Density	Young's Modulus	Friction Coefficient	Poisson Ratio
	1.27 cm	0.843 g/cm^3	10^8 Pa	0.26	0.3
Water	Density	Dynamic Viscosity	Specific Heat	Mass Flow Rate	Outlet Pressure
	0.99 g/cm^3	8.9E-4 Pa·s	4.18E3 J/kg·K	3.6 kg/s	Constant

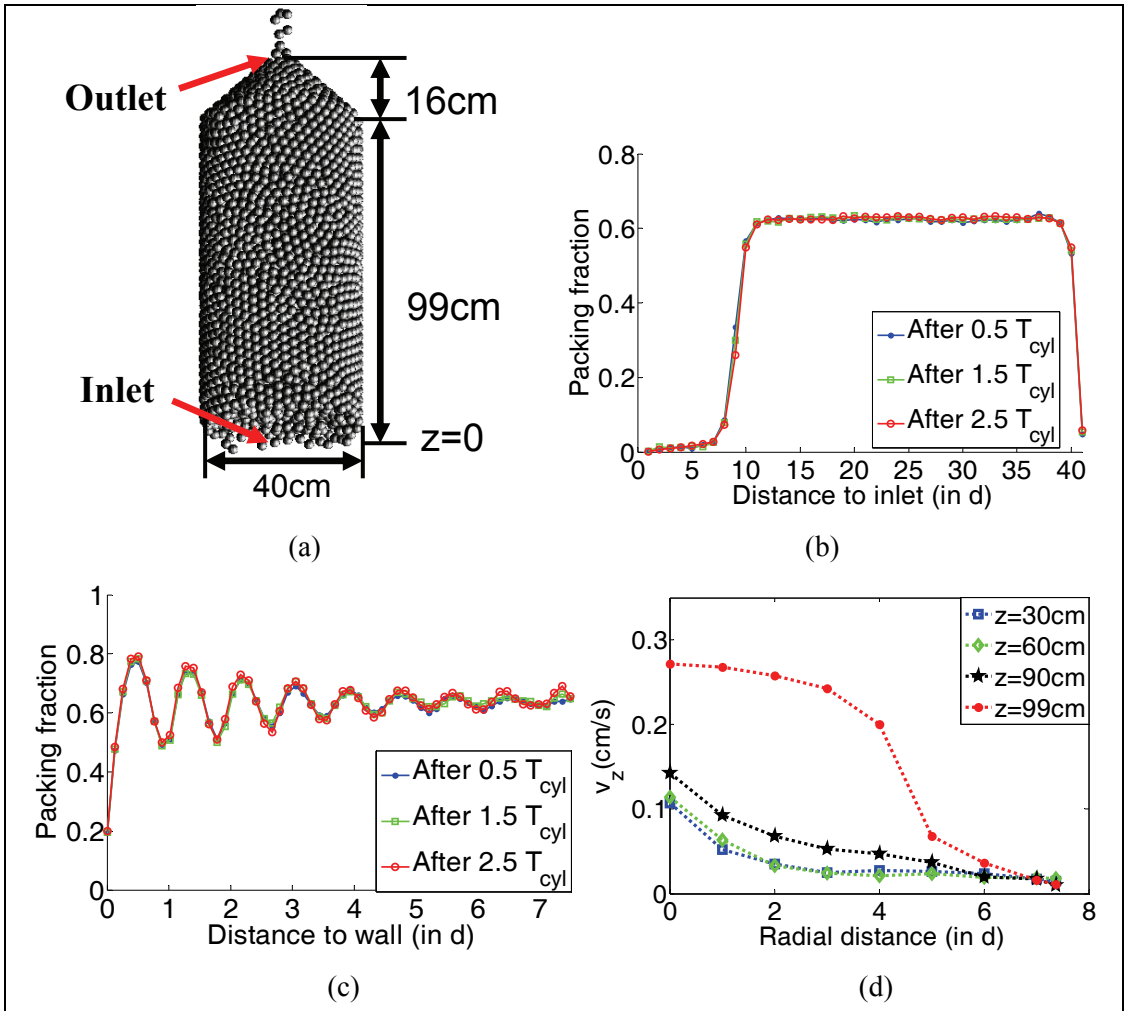

Fig. 2. Scaled PB-AHTR geometry and pebble flow simulation results. (a) Simulation Snapshot; (b) axial packing fraction distribution; (c) radial packing fraction distribution; (d) spatial distribution of v_z.

In the PREX fuel loading, a total of 8300 pebbles are injected from the bottom one by one to fill the core. To start the simulation effectively, a collective pebble packing process is employed in the initial fuel loading modeling. This is done by first generating all the pebbles within the core allowing overlaps using uniform sampling and then by rearranging them and letting them settle down based on a newly developed quasi-dynamics method[23] (QDM). The packing efficiency is greatly enhanced when compared with the sequential landing method. Using the QDM, the initial collective packing can be achieved in <1 min on a PC compared with >10 h for sequential landing. After the initial fuel loading, a recirculation process is simulated by the DEM and CFD solvers. Although the pebble recirculation is a dynamic process that exhibits a stochastic nature, the pebble flow and coolant flow will reach a steady state or a dynamic equilibrium state after enough simulation time. The "dynamic equilibrium state" in this work is defined as a state where the maximum variation of pebble packing fraction over consecutive time steps is less than a threshold (~1%) within any fixed local fluid cell in

the core region. This will yield a <0.1% global variation of pebble packing fraction in the core region. Here we denote T_{cyl} as the average time needed for a pebble to travel from the inlet to the outlet, which is 47 h measured in single-thread CPU time (2600 s measured in physical time) for the PB-AHTR simulation on a Linux-based Dell T7500 3.6GHz workstation. The dynamic equilibrium state can be reached within $0.5T_{cyl}$ from the initial pebble configuration for the PB-AHTR simulation (which is shown in Figs. 2b and 2c), and the simulation stops at $3T_{cyl}$. The final simulation solutions, such as pebble packing fraction distribution, contact stress distribution, coolant pressure distribution, etc., shown in this work are the averaged solutions over a very short time period (~5 s) at the end of simulation time, when the pebble flow and coolant flow are at the dynamic equilibrium state.

The most important pebble flow quantities at the dynamic equilibrium state are pebble density spatial distribution and pebble velocity distribution, as these quantities have a significant impact on the pebble-coolant interaction forces. Also, the pebble density distribution further determines the fission power distribution within the core.

The axial and radial distributions of pebble packing fraction in the scaled PB-AHTR simulation is shown in Figs. 2b and 2c, respectively (the distance is measured by pebble diameter d). It can be seen that the pebble flow can reach its equilibrium state within a half-cycle of the pebble circulation. The axial packing distribution is calculated by uniformly dividing the core into horizontal layers and summing up the pebbles' volume in each layer using the sphere cap volume formula.[24] From Fig. 2b, we can see that within the cylindrical core region, pebbles show near-uniform packing density distribution with the packing fraction of ~63%. Therefore, the uniform packing fraction assumption used in PREX analysis[25] is verified as a good approximation. However, in the PREX analysis, the packing fraction of 0.60 is used, while our result indicates a higher value. The actual packing fraction distribution in PBRs can be experimentally determined though it presents substantial challenges in reality due to the complicated reactor core behavior and limited capability of current measurement techniques. As an alternative, the coupled DEM-CFD simulation with high-fidelity models can alleviate these challenges to some extent and provide realistic values of pebble packing fraction distribution for the further thermal-hydraulic or neutronic analysis, which is one of the motivations of current research.

To calculate the radial distribution of the packing fraction, the core is uniformly divided into annular zones. The packing profile is obtained by counting the accumulative volume of pebbles in each zone using the sphere-cylinder intersection volume formula.[24] The radial packing distribution also tends to be stable within a half-cycle of fuel circulation, like that of the axial profile, except for small fluctuations in the center of the core ($r = 0$). Compared with the static experimental result,[26] we can see that the dynamic pebble flow with coupled fluid interaction has a similar radial packing profile, including the locations and values of the peaks and troughs near the wall. This is because both pebble flow and coolant flow move at a low speed and the whole system can be deemed as quasi-static near the maximally random jamming state.

Since the major force to drive the circulation of pebble and coolant flow is dominant along the axial direction in the system, the radial and azimuthal components of pebble velocity, fluid velocity, and fluid pressure are very small compared to the axial component. Hence, the analysis of pebble and coolant dynamic properties will mainly focus on the axial (z-component) quantity. The z-component velocity profile (azimuthally averaged v_z) of the pebble flow is shown in Fig. 2d. The radial distributions of v_z at different heights of the cylindrical core region are plotted. Figure 2d clearly shows that pebbles with larger radial distance to the center have smaller vertical speed. This is because pebbles bear larger frictions in the region near the wall so the pebble flow becomes slower.[5] When pebbles are closer to the conic region, such as at the entrance of the conic region z = 99 cm shown in Fig. 2d, pebbles move much faster at the central region than at the region near the boundary.

The axial profile of fluid vertical speed (radially and azimuthally averaged u_z) is shown in Fig. 3a. Governed by the fluid mass conservation Eq. (7), the fluid axial speed is almost constant in the pebble bed cylindrical region where the axial distribution of pebble packing fraction is near uniform. By choosing the same material properties as in PREX, our simulation predicts a total hydraulic head loss of Δh_{total} = 5.6 cm water at the top of the cylindrical core region, which is very close to the experimental measurement at Δh_{total} = 5.5 cm water in PREX (Ref. 25). This demonstrates the high fidelity of the developed methodology in simulating the coolant flow for PBRs. The total hydraulic head loss is the difference between total pressure drop Δp_{total} and elevation-induced pressure drop Δp_{elev}, which are plotted as functions of distance to inlet in Fig. 3b.

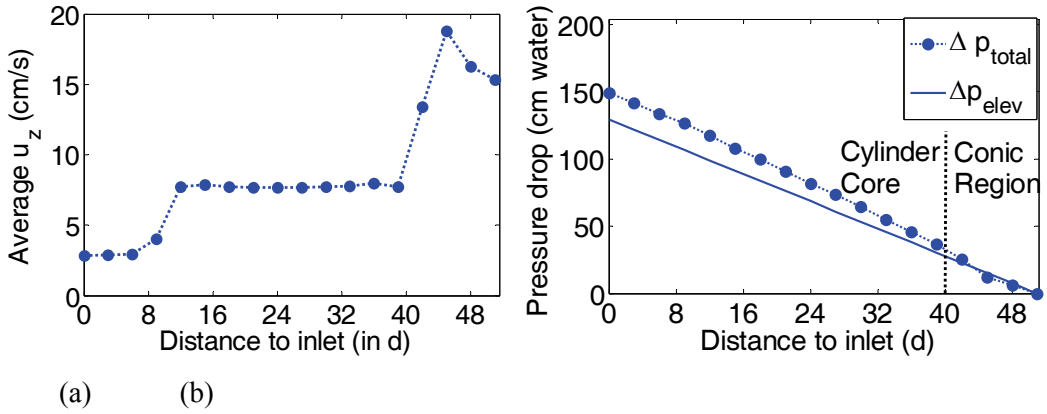

Fig. 3. Axial distribution of flow speed and pressure. (a) Averaged u_z profile along z-axis; (b) averaged pressure drop along z-axis.

III.B. HTR-10 Design Simulation

Different from buoyancy-driven pebble flow in PB-AHTR, gravity-driven pebble flow is present in the helium gas-cooled reactors. A typical design is the HTR-10 reactor system,[17] where the reactor core has a radius of 90 cm (R = 15d) and a height of 252 cm, with a 45-deg conic bottom and

cylindrical chute. In the simulation, a total of 30000 pebbles are randomly generated within the core using the collective dynamics-based initialization algorithm,[23] with the initial packing fraction of ~61%. During recirculation, pebbles are released from the bottom of the reactor through the chute while new pebbles are inserted at the top. Meanwhile, helium gas coolant enters at high pressure from the top and leaves at the bottom, with the boundary conditions of constant velocity inlet and constant pressure outlet. The side view of the reactor is shown in Fig. 4a (generated by ParaView), and the physical parameters for the pebbles and coolant are listed in Table II. Since the thermal effect is not considered in this work, a uniform temperature of $T = 600^{\circ}\mathrm{C}$ is assumed in the HTR-10. The dynamic equilibrium state is reached within $0.5T_{\mathrm{cyl}}$ from the initial configuration, where T_{cyl} is ~10.5 days measured in CPU time (1400 s measured in physical time). The simulation stops at $1.5T_{\mathrm{cyl}}$, and averaged solutions over the last 5 s are obtained.

Table II Pebble and Coolant Physical Properties for HTR-10 Simulation

Pebble	Radius	Mass	Young's Modulus	Friction Coefficient	Poisson Ratio
	3 cm	210 g	10^9 Pa	0.7	0.3
Helium Coolant*	Density	Dynamic Viscosity	Specific Heat	Mass Flow Rate	Outlet Pressure
	1.65 kg/m^3	3.86E-5 Pa·s	5.19E3 J/kg·K	4.32 kg/s	Constant

*at 600 degrees Celsius, 3MPa.

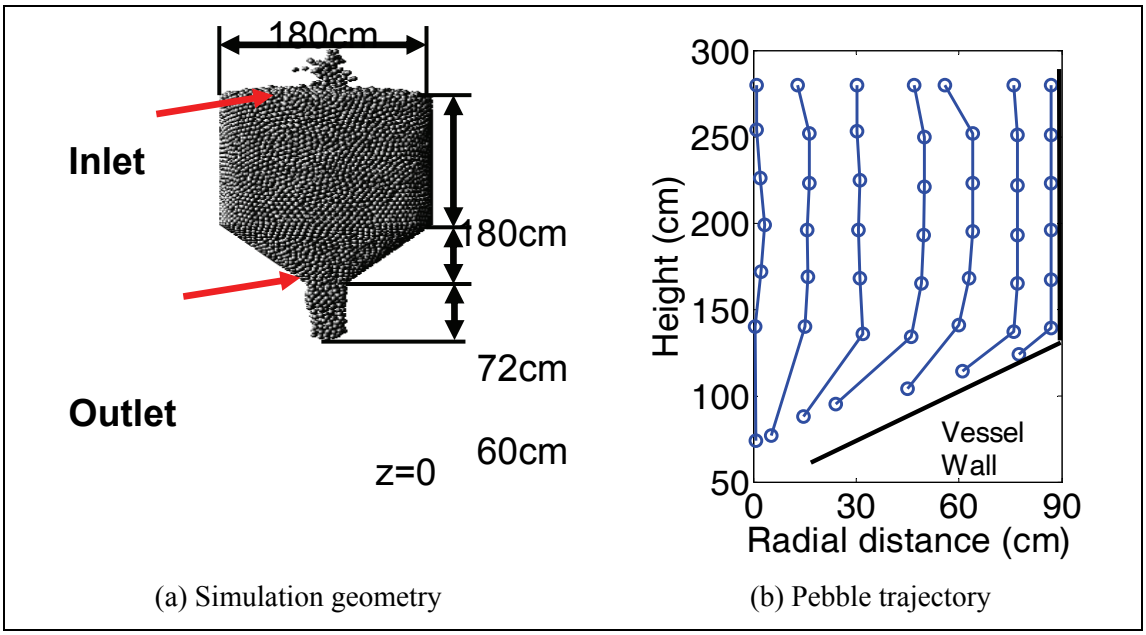

(a) Simulation geometry (b) Pebble trajectory

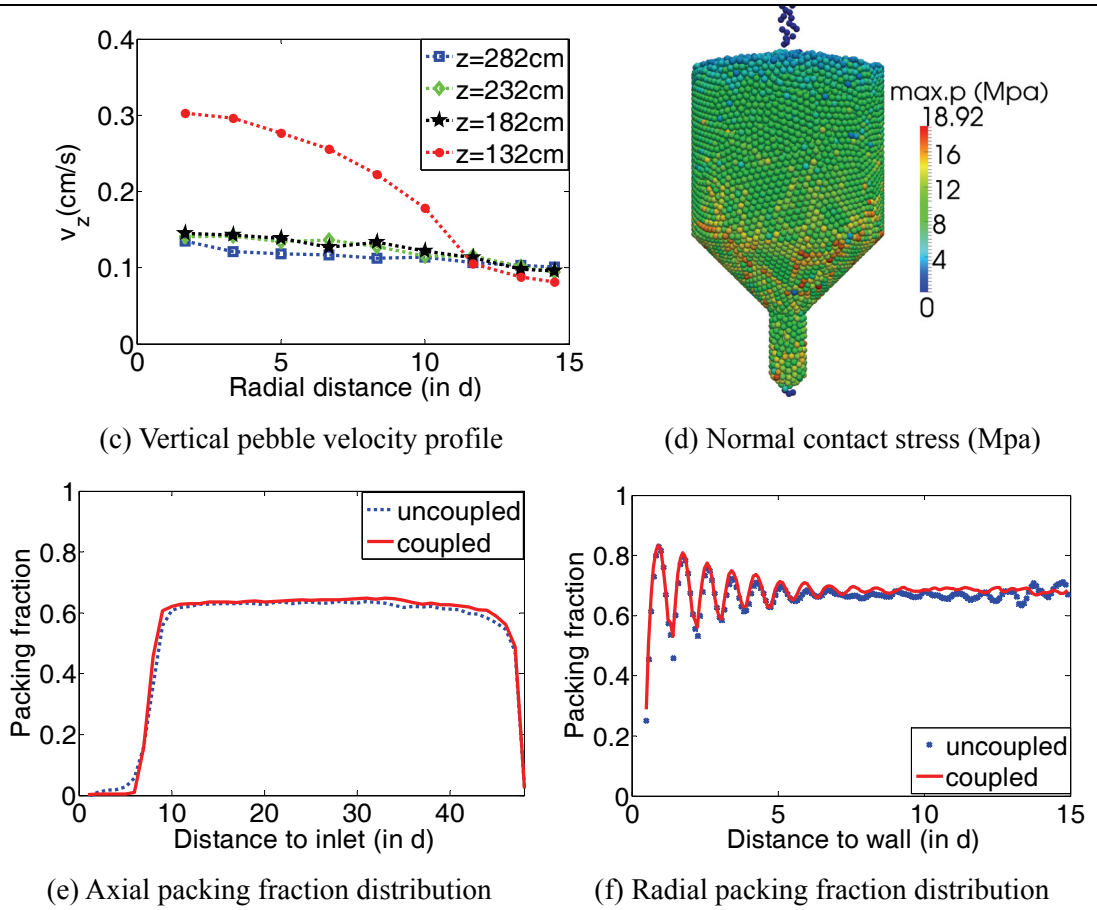

(c) Vertical pebble velocity profile

(d) Normal contact stress (Mpa)

(e) Axial packing fraction distribution

(f) Radial packing fraction distribution

Figure 4. Pebble flow profiles for HTR-10 geometry simulation

Typical pebble trajectories are shown in Fig. 4b. Seven pebbles start at approximately the same height but at different radial positions. The subsequent positions are recorded with equal time increment Δt = 200 s. Although the pebble distribution and interpebble collision have a stochastic nature, the pebble flow exhibits an ordered streamline flow pattern within the core. Moreover, due to the identical time interval between two neighboring recorded positions along a trajectory, Fig. 4b implies that the z-component of the pebble velocity v_z is almost uniform within the cylindrical core region, independent of the radial position except for the region near the wall. For pebbles near the wall, the vertical speed becomes slightly slower due to the higher frictions, as shown in Fig. 4c. Different from the pebble behavior in the cylindrical core region, pebbles within the conic outlet region show faster speeds at small radial positions than at large radial positions, as shown in Fig. 4c at the entrance of the conic region z = 132 cm. In the previous DEM-only simulation for annular geometry by Rycroft et al.,[5] the inner cylindrical guide ring and the pebble flow within the ring have similar cross-sectional geometry as HTR-10 (R = 14.5d). The v_z profile given by Rycroft et al. also exhibits approximate uniformity in the cylindrical region and non-uniformity in the conic region. This shows that the characteristics of pebble trajectory and vertical speed distribution are not changed with

the presence of coolant flow in HTR-10 design.

For HTR-10 or other larger geometries, such as PBMR-400, tens or hundreds of thousands of pebbles are stacked within the reactor core. One crucial design issue is the material strength of the graphite, since the contact stress on the pebbles at the bottom of the reactor could be as high as the graphite maximum yield strength. To investigate this issue, the distribution of the maximum normal contact stress on each pebble throughout the core and the outlet region is calculated and shown in Fig. 4d. The global maximum pebble contact stress can be calculated according to Eq. (16) as follows[18]:

$$\max_{i=1,2,..N}(p_{\mathrm{n,i}}) = \frac{1}{\pi}\left[\frac{6\max(F_{\mathrm{n,i}})E^2}{(1-\nu^2)^2 r^2}\right]^{1/3}, \tag{16}$$

where $F_{\mathrm{n,i}}$ is the normal contact force onto the i^{th} pebble and parameters $E$and ν are the pebble Young's modulus and Poisson ratio, listed in Table II. Figure 4d shows that the global maximum value occurs near the wall close to the top of the conic region, with the stress value of 18.92 MPa, though the mean average contact stress around this region is <10 Mpa. In the molecular dynamics method-based pebble flow simulation (pebble discharge case) by Lee,[9] the global maximum normal contact stress also occurred near this region. As for commercial graphite, the compressive strength has the order of 100 MPa,[27] hence, the material failure of fuel pebbles is not a great concern in the PBR design, at least for the HTR-10 design under the study.

The distribution of pebble packing fraction in the cylindrical core region is shown in Figs. 4e and 4f. The average pebble packing fraction is 63.4%, while this value is 63.0% in the pebble-flow-only simulation result presented by Rycroft et al.[5] To verify this discrepancy, we perform simulations of pebble flow only (using DEM), and the resultant pebble packing fraction distributions are also presented in Figs. 4e and 4f, denoted as "uncoupled solutions." Our uncoupled (DEM-only) simulation shows that an average of packing fraction of 62.9% is obtained, which is consistent with the result presented by Rycroft et al.[5] It can be seen that coupled flow simulations lead to higher packing fraction in the core region and smaller oscillation in radial packing fraction distribution than those predicted by uncoupled pebble flow simulations. This difference can be attributed to the densification effect of the downward helium flow. The drag force from the helium gas provides additional driving force in addition to the gravity on the downward pebble flow and increases the pebble packing density. To substantiate the strong effect from the drag force, a qualitative analysis can be provided. Based on the parameters provided in Table II, it can be calculated that the average superficial speed along the z-direction in HTR-10 is u_0 = 1.03 m/s, and by using the average porosity of ε_0 = 0.366 within the core, the average Reynolds number is $\mathrm{Re} \sim (\rho \cdot u_0 \cdot d \cdot \varepsilon_0/\mu) \sim 1000$. Based on Eq. (14), the average drag force can be estimated as: $F_{D0} \sim 0.5 \cdot 0.44 \cdot \rho \cdot u_0^2 \cdot \varepsilon_0^{-2} \cdot \pi \cdot r^2 \cdot \beta(\varepsilon_0) \sim 0.08$ N. Compared with the gravitational force of a pebble (2.05N), the fluid force cannot be neglected, although it is not as significant as that in the PB-AHTR case.

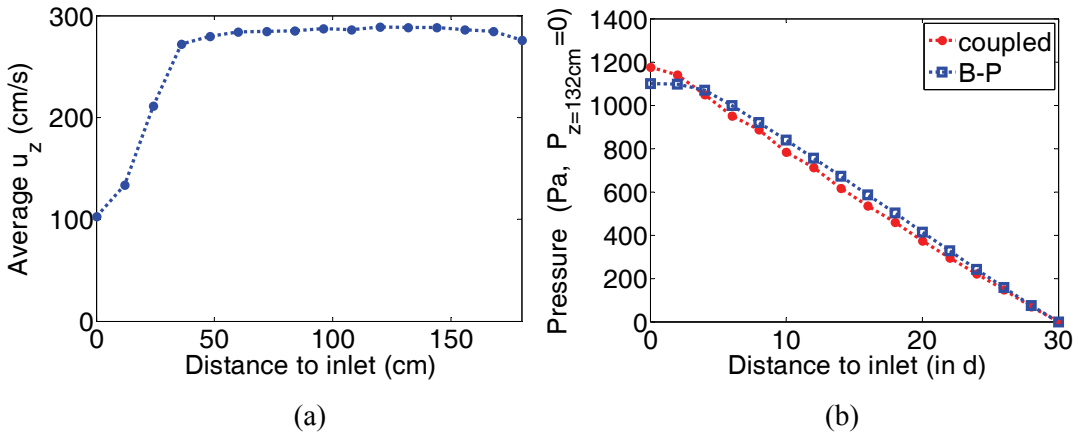

Fig. 5. Axial profile of vertical flow speed and pressure

The axial profiles of coolant vertical flow velocity and pressure drop within the cylinder core are shown in Fig. 5. Similar to the PB-AHTR application, due to the near-uniform axial distribution of pebble packing fraction in the cylindrical core region, the z-direction flow velocity and pressure drop distribution exhibit nearly constant and linear behavior, respectively, in this stable region in the HTR-10 case. Normally, an empirical model based on Burke-Plummer (B-P) equation was used to analyze the helium pressure drop along the axial direction in HTR-10.[17] The B-P equation has been demonstrated as a good approximate model to predict the fluid pressure drop through a packed bed at high Reynolds numbers (Re > 1000).[28] It is written as

$$\frac{\Delta p}{\Delta z} = \frac{1.75\rho \mathrm{u}_0^{\,2}}{\mathrm{d}} \frac{1-\varepsilon}{\varepsilon^3}. \tag{17}$$

To show the high fidelity of the developed tightly coupled multiphysics model, the HTR-10 core pressure drop is calculated based on the B-P equation using the predicted axial porosity distribution from coupled simulations. The solution is shown in Fig. 5b, denoted as "B-P". We can see that the B-P model predicts a similar vertical pressure gradient within the bulk region as the coupled simulation. However, the difference near the inlet region is appreciable. This difference is caused by the fact that the B-P model does not account for the pebble motion, which is much more significant in the region near the inlet than that in the bulk region (~10 cm/s versus ~0.1 cm/s). This comparison shows that the B-P model underestimates the total pressure drop through the reactor core, though the porosity distribution used is from the fully coupled simulation.

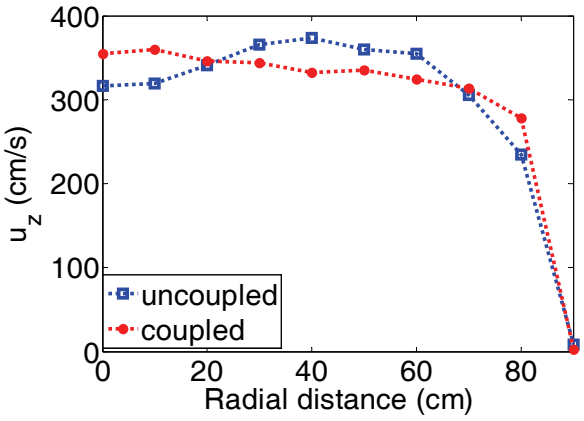

Figure 6. Radial distribution of u_z in HTR-10 simulation

Figures 4e and 4f show that coupling can bring higher pebble packing fractions in the reactor core region due to the fluid forces. Since the pebble-coolant interaction is a two-way effect, the fluid force affects the pebble distribution, and the altered pebble packing density can in turn affect the fluid properties such as the velocity and pressure. To show the coupling effect on the coolant flow behavior, simulations without coupling are performed. First, pebble flow is simulated without the presence of coolant. Then coolant flow is simulated through the pebble bed with pebbles statically packed. The radial distribution of calculated vertical fluid speed u_z at z = 160 cm is compared with the coupled simulation as shown in Fig. 6. It can be seen that the pebble-fluid coupling results in a more uniform and centered vertical velocity distribution compared with the uncoupled approach. One important reason for this discrepancy is the difference in radial packing fraction distribution between the coupled and uncoupled simulations as shown in Fig. 4f: Smaller oscillation behavior of the radial packing fraction distribution in the coupled simulation causes a more uniform and centered distribution of vertical speed of coolant along the radial direction.

IV. CONCLUSIONS

Because of good balance between fidelity and efficiency, the DEM-CFD model is widely used to solve fluid-pebble systems. A fully coupled DEM-CFD methodology based on multiphysics models is developed and applied to model the pebble flow and coolant flow in two types of PBR designs. The coupling of DEM and CFD is realized through the information exchange of fluid-pebble interaction terms.

For the scaled PB-AHTR design, which is based on UC-Berkeley's PREX, the pebble packing fraction distributions in both axial and radial directions are obtained. The pebble packing fractions in the PREX facility can be as high as that of random close packing and do not have significant changes as the recirculation process goes on. This observation indicates that although pebbles move at noticeable speeds, the pebbles in the cylindrical core region are in a stable near-jamming state from the view of packing statistics. The radial distribution of pebble vertical speed is calculated and shows

a maximum value at the center of the core. The speed gradually decreases as the radial distance increases, indicating that the wall friction has a strong impact on the pebbles of the interior region in the PREX facility due to the small core geometry. Axial coolant speed and pressure distributions are also obtained, and the 5.6-cm hydraulic loss in the core region is close to the value of 5.5 cm that is measured in the original experiment. This excellent agreement demonstrates the high fidelity of the developed methodology in analyzing the coolant flow in the PREX facility and shows the potential for application to thermal-hydraulic analysis for PBRs in the future as a practical method.

For the helium gas-cooled HTR-10, the axial and radial distributions of pebble packing fractions are calculated. Typical pebble trajectories for pebbles starting at different radial positions but the same height near the inlet are tracked until these pebbles leave the reactor core region. The trajectories from one time point to the next one with equal time interval are plotted, from which the pebbles' vertical speed distribution can be obtained. Pebble flow presents almost uniform distributions in the pebble vertical speed along both the axial and radial directions within the cylindrical core region, similar to the distributions obtained in the single-phase pebble flow simulations done by other researchers. The radial distribution of the pebble vertical speed is also plotted and shows insignificant difference between the interior and the near-wall region compared to the PB-AHTR simulation. This is due to the relatively larger core size of HTR-10 compared to the scaled PB-AHTR facility. The wall friction has a minor effect on the pebble flow speed at the region near the wall in the HTR-10.

The relatively higher amount of pebbles within a larger geometry also brings the concern of the pebble graphite material strength. The distribution of maximum contact stress on each pebble is calculated in this paper. The results suggest that the global maximum stress occurs near the top wall of the conic outlet region, which agrees with the molecular dynamics-based single-phase pebble flow result. Since this global maximum stress is much less than the compressive yield strength of graphite, the material strength is not a practical concern in PBR designs. The stable and uniform axial pebble packing density in the cylindrical core region leads to almost constant coolant vertical speed and linear vertical pressure variation rate along the axial direction. The coupling effect brings in some noticeable alterations on the pebble packing statistics and fluid properties, such as the slightly higher packing fraction for pebbles due to the fluid-induced densification and more uniform and centered radial distribution of coolant vertical speed.

The computational CPU time for DEM calculations is the dominant factor for the overall simulation efficiency. The computation time for each DEM step is approximately O(N) (Ref. 29). For a larger geometry such as the PBMR-400 design, there are >450000 pebbles within the core. It will take >2 months computational time to simulate one fuel circulation cycle using the developed coupled DEM-CFD methodology on a DELL T7500 3.6-GHz workstation without parallelization. Intensive computational demand is the biggest challenge in pebble flow or coupled pebble flow and coolant flow simulations for larger systems. However, some possible speedup techniques besides parallelization may relieve such a computational burden to some extent. For example, a group of

contiguous pebbles can be treated as a larger rigid coarse sphere,[30] which will significantly reduce the total "sphere number" and hence enhance the simulation efficiency. Because of the quasi-laminar characteristics of the pebble flow, the fidelity loss of this treatment is expected to be insignificant. By combining these available speedup techniques, the CPU time for one fuel circulation cycle simulation in large PBR systems such as the PBMR-400 design could be reduced to be <1 month or even less, which is an acceptable time frame. Future work will focus on the development of simplified models to reduce the heavy computational time in the present DEM-CFD methodology for large PBR system analysis with more physics accounted for, such as thermal effect.

ACKNOWLEDGEMENTS

This work was supported by the U.S. Nuclear Regulatory Commission Faculty Development Grant NRC-38-08-950.

REFERENCES

1. H. D. Gougar and C. B. Davis, "Reactor Pressure Vessel Temperature Analysis for Prismatic and Pebble-bed VHTR Designs," INL/EXE-06-11057, 2006.
2. C. W. Forsberg, P. F. Peterson, and R. A. Kochendarfer, "Design Options for the Advanced High-Temperature Reactor," *Proc. Int. Congress Advances in Nuclear Power Plants (ICAPP '08), Anaheim, California, June 8–12, 2008, American Nuclear Society (2008) (CD-ROM).*
3. P. Bardet, et al., "Design, Analysis and Development of the Modular PB-AHTR," *Proc. Int. Congress Advances in Nuclear Power Plants (ICAPP '08)*, Anaheim, California, June 8–12, 2008, American Nuclear Society (2008) (CD-ROM).
4. A. M. Ougouag, J. Ortensi, and H. Hiruta, "Analysis of an Earthquake-Initiated-Transient in a PBR," *Proceedings of International Conference on Mathematics, Computational Methods and Reactor Physics* (*M&C 2009*), Saratoga Springs, New York, May 3-7, (2009).
5. C. H. Rycroft, et al. "Analysis of Granular Flow in A Pebble Bed Nuclear Reactor," *Phys. Rev. E*, **74**, 021306 (2006).
6. J. J. Cogliati and A. M. Ougouag, "PEBBLES: A Computer Code for Modeling Packing, Flow and Recirculation of Pebbles in a Pebble Bed Reactor," *Proceedings of 3rd International Topical Meeting on High Temperature Reactor Technology*, October 1-4, 2006, Johannesburg, South Africa.
7. H. Park, et al., "Tightly Coupled Multiphysics Algorithms for Pebble Bed Reactors," *Nucl. Sci. Eng.*, **166**, 118-133 (2010).
8. P. A. Cundall and O. D. L. Strack, "A discrete numerical model for granular assemblies," *Geotechnique* **29**, 47-65 (1979).
9. K. Lee, "Particle Tracking using Molecular Dynamics Simulation for Pebble Bed Reactors," PHD dissertation, North Carolina State University (2011).

10. F. Reitsma, et al., "The PBMR steady-state and coupled kinetics core thermal-hydraulics benchmark test problems," *Nuclear Engineering and Design* **236**,657-668 (2006).
11. C.Y. Wen and Y.H. Yu, "Mechanics of fluidization", *A. I. Ch. E.* **62**, 100-111 (1966).
12. R. D. Felice, "The Voidage Function for Fluid-Particle Interaction Systems," *Int. J. Mult. Flow*, **20**, pp. 153-159 (1994).
13. H. P. Zhu, et al., "Discrete particle simulation of particulate systems: Theoretical developments", *Chem. Eng. Sci.* **62**, pp3378-3396 (2007).
14. D. Gidaspow, Multiphase Flow and Fluidization. Academic Press, San Diego (1994).
15. A.J. Parry, et al., "Modeling blockage of particles in conduit constrictions: dense granular suspension flow", *J. of Fluid Eng.* **132**, 011302 (2010).
16. K.D. Kafui, et al., "Discrete particle-continuum fluid modeling of gas-solid fluidized beds", *Chem. Eng. Sci.* **57**, 2395-2140 (2002).
17. Z. Gao and L. Shi, "Thermal Hydraulic Calculation of the HTR-10 for the Initial and Equilibrium Core," *Nuclear Engineering and Design* **218**, pp.51-64(2002).
18. K. L. Johnson, Contact Mechanics, Cambridge University Press (1985).
19. J. Schafer, S. Dippel, and D. E. Wolf, "Force Schemes in Simulation of Granular Materials," *Journal De Physique*, **6**, 5-20 (1996).
20. B. K. Mishra, C. V. R. Murty, "On the Determination of Contact Parameters for Realistic DEM Simulations of Ball Mills," *Powder Technology*, **115**, 290-297 (2001).
21. D. A. Drew, "Mathematical Modeling of Two-phase Flow," *Ann. Rev. Fluid Mech*, **15**: 261-291 (1983).
22. S. V. Patankar, "Numerical heat transfer and fluid flow", Hemisphere, New York (1980).
23. Y. Li and W. Ji, "A Collective Dynamics-based Method for Initial Pebble Packing in Pebble Flow Simulation", *Nuclear Engineering and Design* **250**, pp. 229-236 (2012).
24. F. Lamarche, et al., "Evaluation of the volume of intersection of a sphere with a cylinder by elliptic integrals", *Computer Physics Communications* **59**, pp. 359-369 (1990).
25. A. Griveau, "Modeling and Transient Analysis for the Pebble Bed Advanced High temperature Reactor (PB-AHTR)," MS Project Report, UCBTH-07-001 (2007).
26. R. F. Benenati, C. B. Brosilow, "Void fraction distribution in beds of spheres", *A.I.Ch. E. Journal* **8**, pp. 359-361 (1962).
27. http://www.ceramisis.com/carbons_graphites_specs.htm.
28. D. Nemec and J. Levec, "Flow through packed bed reactors: 1. Single-phase Flow," *Chem. Eng. Sci.* **60**, 6947-6957 (2005),
29. J. J. Cogliati and A. M. Ougouag, "PEBBLES Mechanics Simulation Speedup," *PHYSOR* 2010, Pittsburgh, PA, USA, May 9-14, 2010.
30. M. Sakai, "Large-scale discrete element modeling in a fluidized bed," *Intl. J. Num. Meth. Fluids* **64**, 1319-1335 (2010).